Inorg. Chem. **2008**, *47*, 4844−4853

Preparation, Structures, and Photocatalytic Properties of Three New Uranyl−Organic Assembly Compounds

Zuo-Lei Liao,[†] Guo-Dong Li,[†] Ming-Hui Bi,[†] and Jie-Sheng Chen*[,†,‡]

State Key Laboratory of Inorganic Synthesis and Preparative Chemistry, Jilin University, Changchun 130012, P.R. China, and School of Chemistry and Chemical Technology, Shanghai Jiao Tong University, Shanghai 200240, P.R. China

Received January 21, 2008

Three new uranyl−organic coordination polymers $(UO_2)_8(NDC)_{12}(4,4'\text{-bipyH}_2)_3(4,4'\text{-bipyH})_3$ (**1**), $(UO_2)_3O[Ag(2,2'\text{-bipy})_2]_2(NDC)_3$ (**2**), and $(UO_2)_2(NDC)_2(2,2'\text{-bipy})_2$ (**3**), where NDC = 1,4-naphthalenedicarboxylate and bipy = bipyridine, have been prepared in hydrothermal conditions. Both **1** and **2** possess a 2D structure while **3** is composed of 1D zigzag chains. In **1** there are mononuclear pentagonal-bipyramidal U−O polyhedra and 1D channels filled with 4,4′-bipy molecules, whereas in **2** there are mononuclear hexagonal-bipyramidal U−O polyhedra and tetranuclear pentagonal-bipyramidal U−O clusters which form 2D channels with occluded $[Ag(2,2'\text{-bipy})_2]^+$ counterions. In **3** both the NDC and the bipy ligands coordinate to uranyl centers, leading to hexagonal-bipyramidal polyhedra which are connected to form 1D zigzag chains. Under UV or visible irradiation, **1** and **2** degrade rhodamine B with similar efficiency. The correlation between photocatalytic reaction rate and oxygen concentration for **1** and **2** has also been elucidated. Crystal data: **1**, triclinic, space group $P\bar{1}$, $a = 11.037(2)$ Å, $b = 15.126(3)$ Å, $c = 15.660(3)$ Å, $\alpha = 62.05(3)°$, $\beta = 72.26(3)°$, $\gamma = 82.05(3)°$, and $Z = 2$; **2**, triclinic, space group $P\bar{1}$, $a = 14.161(3)$ Å, $b = 15.122(3)$ Å, $c = 18.212(4)$ Å, $\alpha = 85.73(3)°$, $\beta = 76.99(3)°$, $\gamma = 67.32(3)°$, and $Z = 2$; **3**, monoclinic, space group $P2_1/n$, $a = 10.7976(18)$ Å, $b = 31.501(6)$ Å, $c = 11.590(2)$ Å, $\beta = 97.609(4)°$, and $Z = 4$.

Introduction

The chemistry of metal–organic coordination assemblies has been enriched enormously in the past two decades, and a variety of coordination assembly compounds have been discovered.[1] Most of the assembly compounds reported so far involve d-block transition metals or 4f lanthanide metals as their structure-building units. These assemblies show diverse structural topologies with various dimensions and connections,[2] and interesting properties, such as luminescence,[3] magnetism,[4] gas storage,[5] and catalysis,[6] have been revealed for these compounds.

In comparison with the extensively used d-block and 4f lanthanide metals, the 5f actinide metals are less common

* To whom correspondence should be addressed. E-mail: chemcj@jlu.edu.cn, chemcj@sjtu.edu.cn. Fax: +(86)-(431)-85168624.

† Jilin University.

‡ Shanghai Jiao Tong University.

(1) (a) Moulton, B.; Zaworotko, M. J. *Chem. Rev.* **2001**, *101*, 1629–1658. (b) Eddaoudi, M.; Moler, D. B.; Li, H. L.; Chen, B. L.; Reineke, T. M.; O'Keeffe, M.; Yaghi, O. M. *Acc. Chem. Res.* **2001**, *34*, 319–330. (c) Ockwig, N. W.; Delgado-Friedrichs, O.; O'Keeffe, M.; Yaghi, O. M. *Acc. Chem. Res.* **2005**, *38*, 176–182. (d) Khlobystov, A. N.; Blake, A. J.; Champness, N. R.; Lemenovskii, D. A.; Majouga, A. G.; Zyk, N. V.; Schröder, M. *Coord. Chem. Rev.* **2001**, *222*, 155–192. (e) Evans, O. R.; Lin, W. B. *Acc. Chem. Res.* **2002**, *35*, 511–522. (f) Zhao, X. B.; Xiao, B.; Fletcher, A. J.; Thomas, K. M.; Bradshaw, D.; Rosseinsky, M. J. *Science* **2004**, *306*, 1012–1015. (g) Kitagawa, S.; Kitaura, R.; Noro, S.-I. *Angew. Chem., Int. Ed.* **2004**, *43*, 2334–2375. (h) Férey, G. *Chem. Mater.* **2001**, *13*, 3084–3098. (i) Hagrman, P. J.; Hagrman, D.; Zubieta, J. *Angew. Chem., Int. Ed.* **1999**, *38*, 2638–2684. (j) Rao, C. N. R.; Natarajan, S.; Vaidhyanathan, R. *Angew. Chem., Int. Ed.* **2004**, *43*, 1466–1496.

(2) (a) Bradshaw, D.; Claridge, J. B.; Cussen, E. J.; Prior, T. J.; Rosseinsky, M. J. *Acc. Chem. Res.* **2005**, *38*, 273–282. (b) Férey, G. *Chem. Soc. Rev.* **2008**, *37*, 191–214. (c) Cheetham, A. K.; Rao, C. N. R.; Feller, R. K. *Chem. Commun.* **2006**, 4780–4795. (d) Mandal, S.; Natarajan, S. *Chem.−Eur. J.* **2007**, *13*, 968–977. (e) Tian, Y. Q.; Cai, C. X.; Ji, Y.; You, X. Z.; Peng, S. M.; Lee, G. H. *Angew. Chem., Int. Ed.* **2002**, *41*, 1384–1386. (f) Xiong, R. G.; You, X. Z.; Abrahams, B. F.; Xue, Z. L.; Che, C. M. *Angew. Chem., Int. Ed.* **2001**, *40*, 4422–4425.

(3) (a) Chen, W.; Wang, J. Y.; Chen, C.; Yue, Q.; Yuan, H. M.; Chen, J. S.; Wang, S. N. *Inorg. Chem.* **2003**, *42*, 944–946. (b) Barthelet, K.; Marrot, J.; Riou, D.; Férey, G. *Angew. Chem., Int. Ed.* **2002**, *41*, 281–284. (c) Moulton, B.; Lu, J. J.; Hajndl, R.; Hariharan, S.; Zaworotko, M. J. *Angew. Chem., Int. Ed.* **2002**, *41*, 2821–2824. (d) Wang, X. Y.; Wang, L.; Wang, Z. M.; Gao, S. *J. Am. Chem. Soc.* **2006**, *128*, 674–675. (e) Halder, G. J.; Kepert, C. J.; Moubaraki, B.; Murray, K. S.; Cashion, J. D. *Science* **2002**, *298*, 1762–1765. (f) Gao, E. Q.; Yue, Y. F.; Bai, S. Q.; He, Z.; Yan, C. H. *J. Am. Chem. Soc.* **2004**, *126*, 1419–1429. (g) Osa, S.; Kido, T.; Matsumoto, N.; Re, N.; Pochaba, A.; Mrozinsk, J. *J. Am. Chem. Soc.* **2004**, *126*, 420–421. (h) Yue, Q.; Yang, J.; Li, G. H.; Li, G. D.; Xu, W.; Chen, J. S.; Wang, S. N. *Inorg. Chem.* **2005**, *44*, 5241–5246.

10.1021/ic800109y CCC: $40.75
Published on Web 04/30/2008

in the area of extended coordination assemblies.[7] Recently, the construction of uranyl−organic assemblies has attracted increasing interest, and a number of coordination polymer compounds formed through the connection of uranyl units with various organic ligands have been prepared and structurally characterized.[8] From a structural point of view, the uranyl ion is likely to form U−O (or U−F, U−N) polyhedra, which may be cross-linked by organic and/or inorganic components into chains, sheets, or three-dimensional frameworks.[9] Furthermore, the U−O (or U−F, U−N) polyhedra have strong tendency to polymerize into various polynuclear clusters such as dinuclear, trinuclear, and tetranuclear clusters, infinite chains, or sheets of different local structures.[10] As a result, a very rich structural chemistry may be found for uranyl−organic assembly compounds.[11]

Besides the rich structural features, the uranyl assemblies are attractive because of their photophysical and photochemical properties.[12] Recently, we have reported two examples of U−Zn−organic compounds with photocurrent and photovoltaic responses,[13] whereas a U−Ni−organic and two U−Ag−organic assemblies were found to be photocatalytically active.[14] However, all these uranyl-assembly compounds are bimetallic and contain a second metal ion such as Zn^{2+}, Ni^{2+}, or Ag^{+} apart from the uranyl units, and this may cause additional complexity to the systems when used as photocatalysts. It is still not very clear whether or not the presence of these second metal ions is necessary to the photophysical or photochemical properties of the coordination polymer compounds, or whether or not they can enhance or reduce the performance of the compounds. On the basis of these considerations, we synthesized three uranyl−organic assemblies, one of which contains Ag while the other two are free of the Ag species. The comparison of their photocatalytic activities will be conducive to revealing the role of uranyl and silver ions in photocatalytic reactions. In the meantime, the photocatalytic reactor was designed in such a way that it is feasible to control the oxygen content in the reactor atmosphere, and therefore to elucidate the correlation between catalytic reaction rate and oxygen concentration, which is important for understanding the photocatalytic mechanism further.

Experimental Section

All chemicals were commercially available. Uranyl acetate was recrystallized from hot water, whereas other chemicals were used as received without further purification.

Synthesis of **1**: a mixture of H_2NDC (0.075 g, 0.35 mmol), uranyl acetate (0.09 g, 0.21 mmol), 4,4′-bipyridine (0.38 g, 0.24 mmol), and glycol (3 mL) was dispersed in water (9 mL) and stirred for 3 h in air. The final precursor with a pH value of 4.6 was transferred to and sealed in a 15 mL Teflon-lined autoclave which was subsequently heated at 160 °C for 3 d and then cooled to room temperature at a rate of 10 °C/h. The pH value was 3.9 for the resulting mother liquid. A 0.09 g quantity of pale-yellow block crystals of **1** was obtained after washing with distilled water and drying in air, and the yield of the product was about 60% on the basis of U. Anal. Calcd. for $U_2O_{16}C_{51}H_{32}N_3$: C, 43.17; H, 2.27; N, 2.96. Found: C, 43.55; H, 1.98; N, 2.62%. Parallel syntheses were conducted to obtain a considerable amount of the final product for photocatalytic testing. The peak positions of the powder X-ray diffraction (XRD) pattern (Supporting Information, Figure S1) for the bulk sample of **1** correspond well to those of the pattern

(4) (a) Mahata, P.; Natarajan, S. *Inorg. Chem.* **2007**, *46*, 1250–1258. (b) Yang, J.; Yue, Q.; Li, G. D.; Cao, J. J.; Li, G. H.; Chen, J. S. *Inorg. Chem.* **2006**, *45*, 2857–2865. (c) Müller-Buschbaum, K.; Gomez-Torres, S.; Larsen, P.; Wickleder, C. *Chem. Mater.* **2007**, *19*, 655–659. (d) Yue, Q.; Yang, J.; Li, G. H.; Li, G. D.; Chen, J. S. *Inorg. Chem.* **2006**, *45*, 4431–4439. (e) Vicentini, G.; Zinner, L. B.; Zukerman-Schpector, J.; Zinner, K. *Coord. Chem. Rev.* **2000**, *196*, 353–382. (f) Zhao, B.; Chen, X. Y.; Cheng, P.; Liao, D. Z.; Yan, S. P.; Jiang, Z. H. *J. Am. Chem. Soc.* **2004**, *126*, 15394–15395.

(5) (a) Wang, Z. K.; Heising, J. M.; Clearfield, A. *J. Am. Chem. Soc.* **2003**, *125*, 10375–10383. (b) Mahata, P.; Madras, G.; Natarajana, S. *Catal. Lett.* **2007**, *115*, 27–32. (c) Fujita, M.; Kwon, Y. J.; Washizu, S.; Ogura, K. *J. Am. Chem. Soc.* **1994**, *116*, 1151–1152. (d) Seo, J. S.; Whang, D.; Lee, H.; Jun, S. I.; Oh, J.; Jeon, Y. J.; Kim, K. *Nature* **2000**, *404*, 982–986. (e) Perles, J.; Iglesias, M.; Martín-Luengo, M.-Á.; Monge, Á. M.; Ruiz-Valero, C.; Snejko, N. *Chem. Mater.* **2005**, *17*, 5837–5842.

(6) (a) Rowsell, J. L. C.; Yaghi, O. M. *Angew. Chem., Int. Ed.* **2005**, *44*, 4670–4679. (b) Wong-Foy, A. G.; Matzger, A. J.; Yaghi, O. M. *J. Am. Chem. Soc.* **2006**, *128*, 3494–3495. (c) Pan, L.; Sander, M. B.; Huang, X. Y.; Li, J.; Smith, M.; Bittner, E.; Bockrath, B.; Johnson, J. K. *J. Am. Chem. Soc.* **2004**, *126*, 1308–1309. (d) Dincă, M.; Yu, A. F.; Long, J. R. *J. Am. Chem. Soc.* **2006**, *128*, 8904–8913. (e) Lin, X.; Jia, J. H.; Zhao, X. B.; Thomas, K. M.; Blake, A. J.; Walker, G. S.; Champness, N. R.; Hubberstey, P.; Schröder, M. *Angew. Chem., Int. Ed.* **2006**, *45*, 7358–7364.

(7) Frisch, M.; Cahill, C. L. *Dalton Trans.* **2005**, 1518–1523.

(8) (a) Ok, K. M.; Doran, M. B.; O'Hare, D. *J. Mater. Chem.* **2006**, *16*, 3366–3368. (b) Xie, Y. R.; Zhao, H.; Wang, X. S.; Qu, Z. R.; Xiong, R. G.; Xue, X.; Xue, Z. L.; You, X. Z. *Eur. J. Inorg. Chem.* **2003**, 3712–3715. (c) Borkowski, L. A.; Cahill, C. L. *Inorg. Chem.* **2003**, *42*, 7041–7045. (d) Wang, C. M.; Liao, C. H.; Chen, P. L.; Lii, K. H. *Inorg. Chem.* **2006**, *45*, 1436–1438.

(9) (a) Thuéry, P. *Chem. Commun.* **2006**, 853–855. (b) Wang, C. M.; Wu, Y. Y.; Chen, P. L.; Lii, K. H. *Dalton Trans.* **2007**, 1034–1037. (c) Ok, K. M.; Doran, M. B.; O'Hare, D. *Dalton Trans.* **2007**, 3325–3329. (d) Almond, P. M.; Albrecht-Schmitt, T. E. *Inorg. Chem.* **2002**, *41*, 5495–5501. (e) Forbes, T. Z.; Goss, V.; Jain, M.; Burns, P. C. *Inorg. Chem.* **2007**, *46*, 7163–7168. (f) Wang, X. Q.; Huang, J.; Jacobson, A. J. *J. Am. Chem. Soc.* **2002**, *124*, 15190–15191.

(10) (a) Zheng, Y. Z.; Tong, M. L.; Chen, X. M. *Eur. J. Inorg. Chem.* **2005**, 4109–4117. (b) Jiang, Y. S.; Yu, Z. T.; Liao, Z. L.; Li, G. H.; Chen, J. S. *Polyhedron* **2006**, *25*, 1359–1366. (c) Knopeand, K. E.; Cahill, C. L. *Inorg. Chem.* **2007**, *46*, 6607–6612. (d) Kim, J. Y.; Norquist, A. J.; O'Hare, D. *Chem. Mater.* **2003**, *15*, 1970–1975. (e) Li, Y. P.; Cahill, C. L.; Burns, P. C. *Chem. Mater.* **2001**, *13*, 4026–4031. (f) Duval, P. B.; Burns, C. J.; Clark, D. L.; Morris, D. E.; Scott, B. L.; Thompson, J. D.; Werkema, E. L.; Jia, L.; Andersen, R. A. *Angew. Chem., Int. Ed.* **2001**, *40*, 3357–3361.

(11) (a) Alekseev, E. V.; Krivovichev, S. V.; Depmeier, W. *Angew. Chem., Int. Ed.* **2008**, *47*, 549–551. (b) Krivovichev, S. V.; Kahlenberg, V.; Tananaev, I. G.; Kaindl, R.; Mersdorf, E.; Myasoedov, B. F. *J. Am. Chem. Soc.* **2005**, *127*, 1072–1073. (c) Shvareva, T. Y.; Skanthakumar, S.; Soderholm, L.; Clearfield, A.; Albrecht-Schmit, T. E. *Chem. Mater.* **2007**, *19*, 132–134. (d) Cahill, C. L.; de Lill, D. T.; Frisch, M. *CrystEngComm* **2007**, *9*, 15–26. (e) Krivovichev, S. V.; Kahlenberg, V.; Avdontseva, E. Y.; Mersdorf, E.; Kaindl, R. *Eur. J. Inorg. Chem.* **2005**, 1653–1656. (f) Morss, L. R.; Edelstein, N. M.; Fuger, J. *The Chemistry of Actinide and Transactinide Elements*, 3rd ed.; Springer: Dordrecht, 2006; Vol. *4*, Chapter 22, pp 2436−2467.

(12) (a) Grohol, D.; Clearfield, A. *J. Am. Chem. Soc.* **1997**, *119*, 4662–4668. (b) Borkowski, L. A.; Cahill, C. L. *Cryst. Growth Des.* **2006**, *6*, 2241–2247. (c) Borkowski, L. A.; Cahill, C. L. *Cryst. Growth Des.* **2006**, *6*, 2248–2259. (d) Morss, L. R.; Edelstein, N. M.; Fuger, J. *The Chemistry of Actinide and Transactinide Elements*, 3rd ed.; Springer: Dordrecht, 2006; Vol. *1*, Chapter 5, pp 624−630.

(13) (a) Yu, Z. T.; Li, G. D.; Jiang, Y. S.; Xu, J. J.; Chen, J. S. *Dalton Trans.* **2003**, 4219–4220. (b) Chen, W.; Yuan, H. M.; Wang, J. Y.; Liu, Z. Y.; Xu, J. J.; Yang, M.; Chen, J. S. *J. Am. Chem. Soc.* **2003**, *125*, 9266–9267.

(14) (a) Yu, Z. T.; Liao, Z. L.; Jiang, Y. S.; Li, G. H.; Li, G. D.; Chen, J. S. *Chem. Commun.* **2004**, 1814–1815. (b) Yu, Z. T.; Liao, Z. L.; Jiang, Y. S.; Li, G. H.; Chen, J. S. *Chem.—Eur. J.* **2005**, *11*, 2642–2650.

simulated on the basis of the single crystal structure, confirming the phase purity of the product.

The synthesis procedure for compounds **2** and **3** was similar to that of **1**. For **2**, the reaction mixture consisted of H_2NDC (0.085 g, 0.38 mmol), uranyl acetate (0.105 g, 0.25 mmol), 2,2′-bipyridine (0.080 g, 0.51 mmol), $AgNO_3$ (0.080 g, 0.47 mmol), and water (12 mL). A 0.095 g quantity of the final product was obtained with a yield of about 50% based on U. Anal. Calcd. for $U_3Ag_2O_{19}C_{76}H_{50}N_8$: Ag, 9.35; C, 39.55; H, 2.18; N, 4.85. Found: Ag, 8.87; C, 39.79; H, 1.88; N, 4.61%. Again the powder XRD pattern of **2** confirms the phase purity of the sample (Supporting Information, Figure S2). For **3**, the reactants were H_2NDC (0.040 g, 0.19 mmol), uranyl acetate (0.106 g, 0.25 mmol), 2,2′-bipyridine (0.070 g, 0.45 mmol), and water (12 mL). The yield for **3** was rather poor, and a considerable amount of amorphous species was observed in the final reaction system. The crystals of **3** were picked manually under a microscope for powder XRD (Supporting Information, Figure S3), elemental and spectroscopic analysis. Anal. Calcd. for $U_2O_{12}C_{44}H_{28}N_4$: C, 41.30; H, 2.21; N, 4.38. Found: C, 41.51; H, 2.00; N, 4.12%. The pH values of the reaction mixtures and the resulting mother liquors were 4.3 and 2.2 for **2** and 4.7 and 4.3 for **3**, respectively.

The crystallographic data of compounds **1** and **2** were collected on a Rigaku RAXIS-RAPID single-crystal diffractometer equipped with a narrow-focus, 5.4-kW sealed-tube X-ray source (graphite-monochromated Mo Kα radiation with $\lambda = 0.71073$ Å) at room temperature. The data processing was accomplished with the PROCESS-AUTO processing program. Crystallographic data for **3** were recorded at room temperature on a Bruker-AXS Smart CCD diffractometer equipped with a normal-focus, 2.4-kW X-ray source (graphite-monochromated Mo Kα radiation with $\lambda = 0.71073$ Å) operating at 50 kV and 40 mA with increasing ω. All of the structures were solved by direct methods using the program *SHELXS-97*[15] and refined by full-matrix least-squares techniques against F^2 using the *SHELXTL-97*[16] crystallographic software package. All non-H atoms were easily found from the difference Fourier map and refined anisotropically, whereas the H atoms of the organic molecules were placed by geometrical considerations and were added to the structure factor calculation. For compound **1** the protons attached to nitrogen atoms in 4,4′-bipy were also found from the difference Fourier map.

The C, H, and N elemental analysis was performed on a Flash EA 1112 elemental analyzer, whereas the Ag content was determined on a Perkin-Elmer Optima 3300DV ICP spectrometer. The powder XRD data were collected on a Siemens D5005 diffractometer with Cu Kα radiation ($\lambda = 1.5418$ Å) over the 2θ range of 4−40° at room temperature. The solid diffuse reflectance UV/vis spectra were recorded on a Shimadzu UV 3600 spectrometer, whereas the UV/vis spectra for solution samples were obtained on a Shimadzu UV 2450 spectrometer.

Photocatalytic experiments in aqueous solutions were performed in a 500 mL water-cooled quartz cylindrical vessel (Supporting Information, Figure S4). The reaction mixture in the vessel was maintained at room temperature through a continuous flow of water through an external cooling coil. The UV light source was a 400 W high-pressure mercury lamp (main output 313 nm), and the visible light source was a 500 W Xe lamp (main output >400 nm). A suspension of powdered catalyst (500 mg) in fresh aqueous solution of rhodamine B (RhB, 500 mL, 50 ppm) was ultrasonicated for 5 min and magnetically stirred in the dark for at least 30 min (to establish an adsorption/desorption equilibrium of RhB on the sample surface) in the vessel before irradiation. At given irradiation time intervals, a series of aqueous solutions of a certain volume were collected and filtered through micropore filters to remove suspended catalyst particles and then subjected to spectroscopic measurement on the UV/vis spectrometer. The dye concentration was estimated by the absorbance at 552 nm. Because the molar absorptivity of the dye was very high, the sample was diluted to accurately quantify the dye concentration before filtration. A continuous purging gas flow was introduced into the reaction suspension 20 min ahead of and during irradiation to maintain a constant O_2/N_2 ratio in the atmosphere as desired.

Results and Discussion

The crystallographic refinement results are summarized in Table 1. Selected bond lengths and angles for compounds **1**, **2**, and **3** are listed in the Supporting Information, Tables S1, S2 and S3, respectively. Compound **1** crystallizes in 2D layers, which consist of uranium−oxygen pentagonal bipyramids and NDC spacers lying on general positions (Figure 1). Each uranium atom is bound axially to two uranyl oxygen atoms at an average distance of 1.759 Å to form the linear UO_2^{2+}cation. Equatorially, the uranyl cation is chelated to one carboxylate group and bound to three others in a monodentate mode, with an average U−O separation of 2.387 Å. Two distinct NDC linkers are observed within **1**. One bridges two adjacent uranium−oxygen pentagonal bipyramids into a pair through one carboxylate group, and connects to another through one oxygen donor in the other carboxylate group, leaving one oxygen donor unbound. The other one exhibits a chelating mode for both functional groups. The overall structure may be described as layers formed through cross-linking of uranyl–NDC double chains parallel to the *a* axis (Figure 2a). The chains consist of alternate uranium−oxygen pentagonal bipyramid pairs and double bridging NDC linkers. All NDC linkers in the chains adopt a similar coordination fashion. Each double NDC linker connects two adjacent pairs, with three binding positions for each pair. The chelating NDC molecules, on the other hand, cross-link adjacent double chains into infinite layers. Consequently, within the layers, eight-membered apertures are generated by every four uranium−oxygen bipyramids, two chelating NDC and two bridging NDC ligands, with dimensions of 3.1 × 6.5 Å (defined by the shortest O−O contacts). In each layer, the naphthalene rings extend on the same side, and therefore, operated against the inversion center, the layers are packed face to face (the naphthalene side) and back to back (the other side) alternately. The interlayer separation is about 8.0 Å for the face to face layers and 4.8 Å for the back to back layers (between the planes defined by uranium atoms), respectively (Figure 2b). The apertures, on the other hand, are packed into 1D channels along the [-110] direction, in which the partially protonated 4,4′-bipy species (three protons for every two 4,4′-bipy molecules) are located and interact with the NDC naphthalene rings through face-to-edge π-π stacking (Figure 3). Face-to-face π-π stacking is also found between the adjacent bridging NDC ligands within the same layer. Although different from the channels in 3D

(15) Sheldrick, G. M. *SHELXS-97, Programs for X-ray Crystal Structure Solution*; University of Göttingen: Göttingen, Germany, 1997.
(16) Sheldrick, G. M. *SHELXL-97, Programs for X-ray Crystal Structure Refinement*; University of Göttingen: Göttingen, Germany, 1997.

Table 1. Crystallographic Data and Structure Refinement for **1**, **2**, and **3**

compound	**1**	**2**	**3**
empirical formula	$U_2O_{16}C_{51}H_{32}N_3$	$U_3Ag_2O_{19}C_{76}H_{50}N_8$	$U_2O_{12}C_{44}H_{28}N_4$
formula weight	1418.86	2308.06	1279.76
T [K]	293(2)	293(2)	293(2)
space group	$P\bar{1}$ (No. 2)	$P\bar{1}$ (No. 2)	$P2_1/n$ (No. 14)
a [Å]	11.037(2)	14.161(3)	10.7976(18)
b [Å]	15.126(3)	15.122(3)	31.501(6)
c [Å]	15.660(3)	18.212(4)	11.590(2)
α [deg]	62.05(3)	85.73(3)	90
β [deg]	72.26(3)	76.99(3)	97.609(4)
γ [deg]	82.05(3)	67.32(3)	90
V [Å^3]	2199.5(8)	3505.8(12)	3907.5(12)
Z	2	2	4
ρ [g cm^{-3}]	2.142	2.186	2.175
F(000)	1342	2166	2396
μ [mm^{-1}]	7.437	7.536	8.352
θ range [deg]	3.05−27.48	3.06−27.46	1.29−28.39
limiting indices	$14 \le h \le 13$	$-18 \le h \le 18$	$-14 \le h \le 14$
	$-19 \le k \le 19$	$-18 \le k \le 19$	$-24 \le k \le 41$
	$-20 \le l \le 20$	$-23 \le l \le 23$	$-14 \le l \le 15$
reflections collected/unique	21318/9881	33365/15666	28480/9752
R(int)	0.0318	0.0343	0.1395
data/parameters	9881/657	15666/973	9752/559
GOF on F^2	1.039	1.057	0.954
R1 [$I > 2\sigma(I)$][a]	0.0263	0.0347	0.0583
wR2	0.0503	0.0911	0.1356
R (all data), R1	0.0369	0.0509	0.0998
wR2	0.0533	0.1135	0.1593
largest diff. peak/hole [e Å^{-3}]	0.855/−0.826	1.022/−1.231	4.474/−3.412

[a] $R1 = \sum||F_0| - |F_c||/\sum|F_0|$, $wR2 = [\sum w[(F_0^2 - F_c^2)^2/\sum w(F_0^2)^2]^{1/2}$.

porous materials in topology, the channels in packed layered compounds sometimes are still able to be evacuated to accommodate guest molecules.[17] However, possibly owing to the electrostatic interactions and the relative strong π-π stacking between the 4,4′-bipy species and frameworks (approximately 3.3 Å separation between the rings in contact), removal of the 4,4′-bipy species from the channels in compound **1** was not successful.

Compound **2** also bears a 2D structure, which consists of eight-coordinated uranium−oxygen hexagonal bipyramids, and seven-coordinated tetranuclear uranium−oxygen clusters and NDC linkers (Figure 4). Within the hexagonal bipyramidal coordination sphere of uranium, there are two distinct types of oxygens. The terminal oxygens are bonded to the uranium atom from axial directions, with an average U−O separation of 1.752 Å. Six equatorial positions contain three carboxylate groups, all of which are in chelating mode.

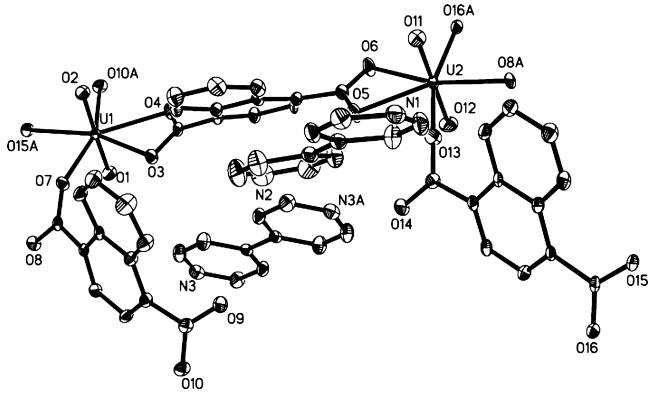

Figure 1. Building block including the asymmetric unit present in **1**. Thermal ellipsoids are drawn at 30% probability, and the hydrogen atoms are omitted for clarity.

Therefore, each hexagonal bipyramid serves as a 3-connected node and connects to three tetranuclear uranium−oxygen clusters through three NDC molecules (Figure 5a). The tetramer, on the other hand, is built up of four pentagonal bipyramids, which join together through three common edges in a planar geometry and lies on the inversion center of the structure. Three types of oxygens are observed within the tetramer: six uranyl oxygens (average U−O separation: 1.772 Å), twelve carboxylate oxygens from six carboxylate groups (average U−O separation: 2.462 Å), and two μ_3-oxygens (average U−O separation: 2.250 Å). All of the outer coordination sites of the tetramer are occupied by carboxylate groups, and each of the tetramers further connects to six hexagonal bipyramids, resulting in a 6-connected node in the 2D network. Therefore, six eight-membered rings are formed around each tetramer, every of which involves two tetramers, two monomers, and four NDC linkers. Operated against the inversion center, they can be divided into three types with different aperture size: 8.4 × 8.6 Å, 7.7 × 10.5 Å, and 0.4 × 10.2 Å (shortest C−C contact). The larger two further pack into straight channels along the b and c axes (Figure 6). It should be pointed out that the layers are not flat. Instead, because the tetramer-NDC-monomer rings are arranged in a chair conformation, the layers are twisted into a wave-like configuration to accommodate one another (Figure 5b and 5c). The Ag^+ ions, on the other hand, are chelated by 2,2′-bipy ligands in a distorted tetrahedral geometry (average Ag−N bond length of 2.339 Å and bond angles ranging from 69.6 ° to 146.4 °) and are located in the channels to balance the negative charges of the

(17) (a) Davies, R. P.; Less, R. J.; Lickiss, P. D.; White, A. J. P. *Dalton Trans.* **2007**, 2528–2535. (b) Kaneko, W.; Ohba, M.; Kitagawa, S. *J. Am. Chem. Soc.* **2007**, *129*, 13706–13712.

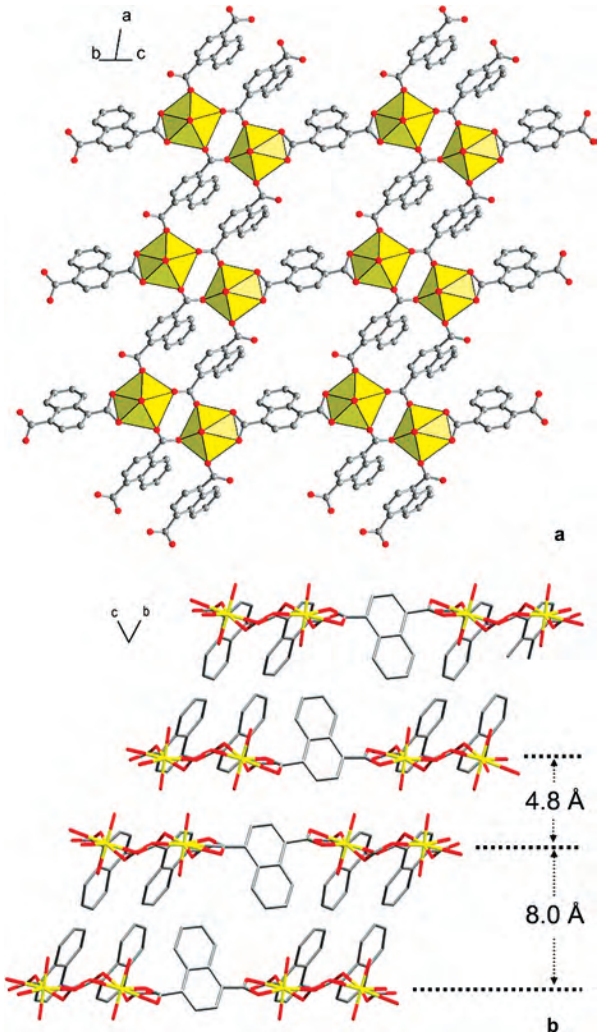

Figure 2. Uranyl−organic layer in **1** viewed along the [011] direction (a), and the layers viewed along the *a* axis showing the "face-to-face" and "back-to-back" packing (b). The 4,4′-bipy species are omitted for clarity.

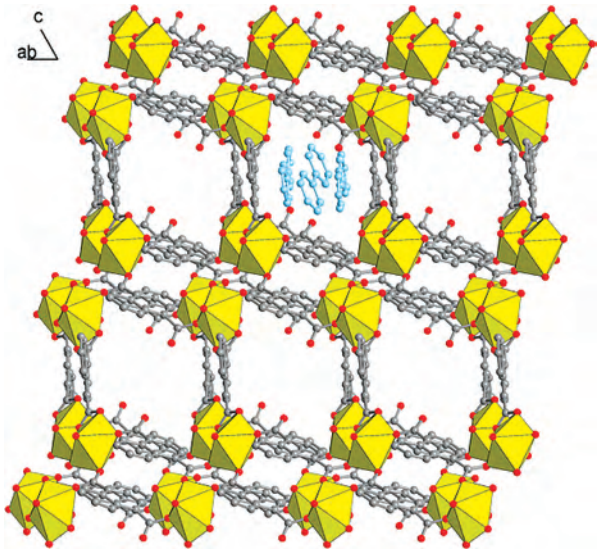

Figure 3. Channels in **1** viewed along the [-110] direction. For clarity, the 4,4′-bipy species are illustrated in only one channel.

uranyl–NDC layers. In inorganic framework construction, the metal–organic complexes are able to template the

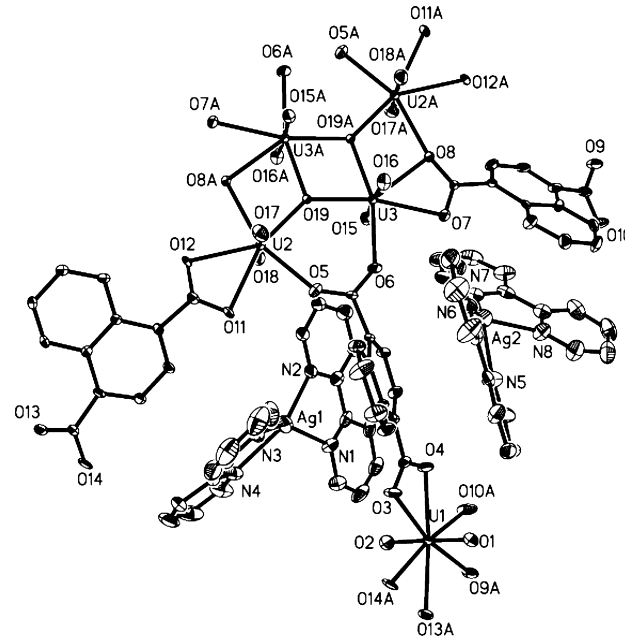

Figure 4. Building block including the asymmetric unit present in **2**. Thermal ellipsoids are drawn at 30% probability, and the hydrogen atoms are omitted for clarity.

formation of a series of metal phosphates,[18] and complex counterions have also been found in a number of coordination assemblies.[19] Recently, Thuéry successfully synthesized a Cu−U−organic compound which consists of copper–bipy backbones incorporated with uranyl−organic coordination counterions.[20] Thus, our discovery completes the three typical arrangements regarding the uranyl and transition metal species in bimetallic uranyl-containing assemblies: hetero-metal–organic architectures, transition metal–organic backbones with uranyl complex guests, and uranyl−organic backbones with transition metal complex guests. In **2**, besides electrostatic interactions, the $Ag(2,2'\text{-bipy})_2^+$ species interact with uranyl−organic layers through face-to-face π-π stacking between NDC and bipy rings. Meanwhile, face-to-face π-π stacking is also found between NDC aromatic rings from adjacent layers.

One interesting feature of **2** is the coexistence of both tetranuclear and mononuclear uranyl units within the same compound. This is an unusual structural feature that significantly distinguishes **2** from the recent example involving uranyl and NDC ligands, in which all uranyl ions are eight-coordinated monomers at equal crystallographic positions, forming a layered (6,3)-network.[21] The polymerization of

(18) (a) Morgan, K. R.; Gainsford, G. J.; Milestone, N. B. *Chem. Commun.* **1997**, 61–62. (b) Williams, D. J.; Kruger, J. S.; McLeroy, A. F.; Wilkinson, A. P.; Hanson, J. C. *Chem. Mater.* **1999**, *11*, 2241–2249.
(19) (a) Rusanova, J. A.; Domasevitch, K. V.; Vassilyeva, O. Y.; Kokozay, V. N.; Rusanov, E. B.; Nedelko, S. G.; Chukova, O. V.; Ahrens, B.; Raithby, P. R. *J. Chem. Soc., Dalton Trans.* **2000**, 2175–2182. (b) Colacio, E.; Kivekäs, R.; Lloret, F.; Sunberg, M.; Suarez-Varela, J.; Bardají, M.; Laguna, A. *Inorg. Chem.* **2002**, *41*, 5141–5149.
(20) Thuéry, P. *CrystEngComm* **2007**, *9*, 358–360.
(21) Go, Y. B.; Wang, X. Q.; Jacobson, A. J. *Inorg. Chem.* **2007**, *46*, 6594–6600.

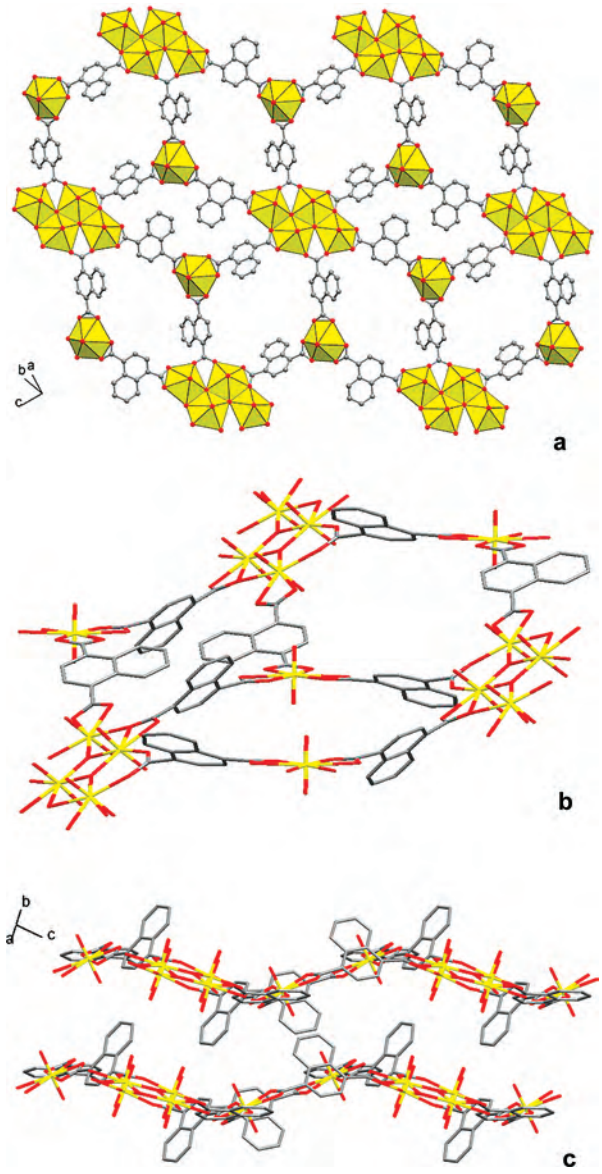

Figure 5. Uranyl−organic layer (a), the eight-membered apertures in chair conformation (b), and the wave-like configuration of layers (c) in **2**. The $[Ag(2,2'\text{-bipy})_2]^+$ species are omitted for clarity.

metal ions is highly dependent on the acidity in solution.[22] Therefore, it is not surprising to find that in most cases the uranyl species are either isolated monomers or polymerized into the same clusters in one compound.[7–11,13,14] However, because of the complexity of hydrothermal reaction systems, the details of the crystallization processes are still far from clear, and apart from the acidity, the temperature, the ion concentration, and the nature of ligand may also play a role in controlling the polymerization to a considerable extent. In the case of **2**, in addition, the pH value fell from 4.4 to 2.2 after the hydrothermal reaction, a much more distinct

(22) (a) Clark, D. L.; Conradson, S. D.; Donohoe, R. J.; Keogh, D. W.; Morris, D. E.; Palmer, P. D.; Rogers, R. D.; Tait, C. D. *Inorg. Chem.* **1999**, *38*, 1456–1466. (b) Palmer, D. A.; Nguyen-Trung, C. *J. Solution Chem.* **1995**, *24*, 1281–1291. (c) Bases, C. F., Jr; Mesmer R. E. *The Hydrolysis of Cations*; John Wiley & Sons: New York, 1976; Chapter 9, pp 174−182. (d) Morss, L. R.; Edelstein, N. M.; Fuger, J. *The Chemistry of Actinide and Transactinide Elements*, 3rd ed.; Springer: Dordrecht, 2006; Vol. *4*, Chapter 23, pp 2553−2556.

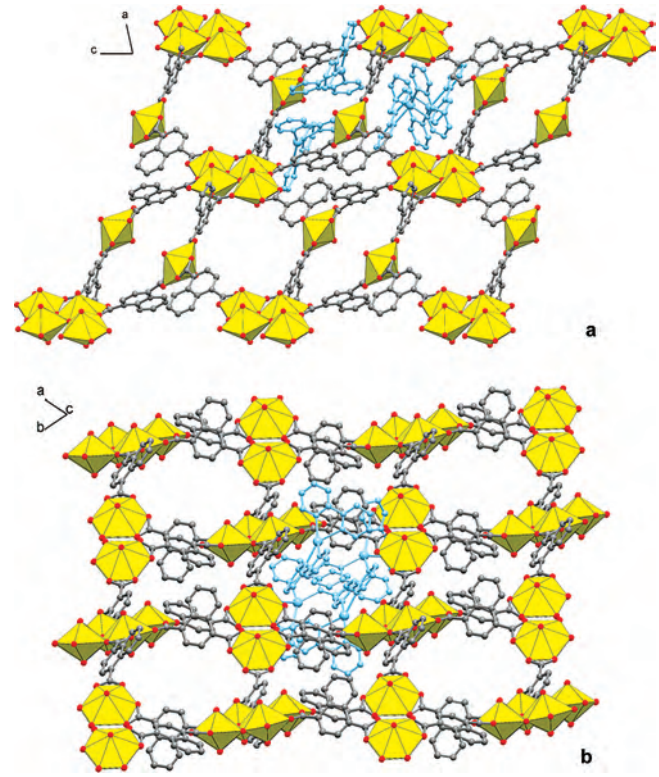

Figure 6. Channels in **2** viewed along the *b* axis (a) and along the *c* axis (b). The $[Ag(2,2'\text{-bipy})_2]^+$ species are illustrated only in distinct channels.

change than those for **1** and **3**. This marked pH variation may also be correlated with the unusual polymerization in the final product of **2**.

Compound **3** crystallizes in 1D chains. It contains two crystallographically independent uranyl sites, both of which are in similar hexagonal bipyramids coordination environments (Figure 7). The uranyl oxygens for U1 are in typical positions, with an average U−O separation of 1.770 Å and a bond angle of 178.4 °. The equatorial plane is defined by two chelating carboxylate groups from two NDC molecules, in a typical range for U−O contact: from 2.448 Å to 2.483 Å. The coordination sphere is completed by an additional 2,2′-bipy molecule in chelating mode (average U−N separation 2.625 Å), with the two nitrogen donors being located slightly out of the mean plane defined by the O-donors. One nitrogen donor is positioned about 0.9 Å from the one side of the plane while the other is about 0.5 Å from the other side. Therefore, a twisted hexagonal bipyramid is formed for U1. The coordination for U2 is almost the same as for U1, except for some minor variations in bond lengths and angles as summarized in Supporting Information, Table S3. All the NDC ligands adopt the same chelating coordination fashion for their carboxylate groups. Every NDC ligand bridges two uranyl centers, resulting in zigzag uranyl−organic chains along the *b* axis (Figure 8). The chains are then packed together through face-to-face π-π stacking between NDC and bipy rings from adjacent chains.

All three compounds involve NDC and bipy ligands, but only in **3** do the bipy moieties coordinate to the uranyl center. It has been demonstrated in many reported compounds that

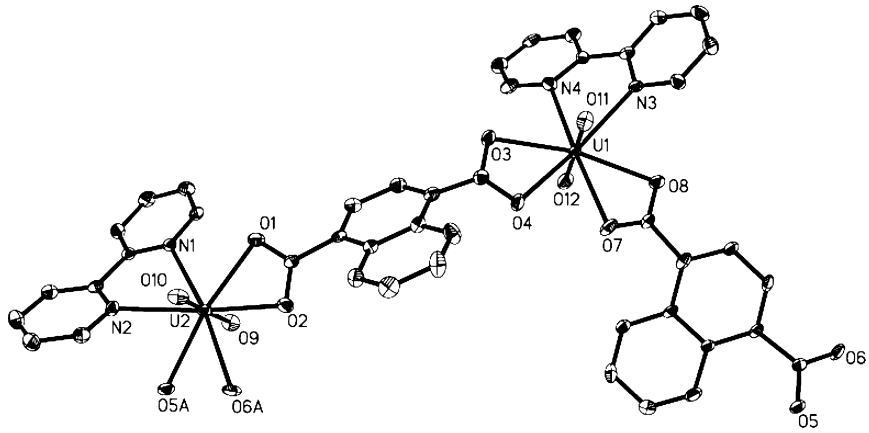

Figure 7. Building block including the asymmetric unit present in **3**. Thermal ellipsoids are drawn at 30% probability, and the hydrogen atoms are omitted for clarity.

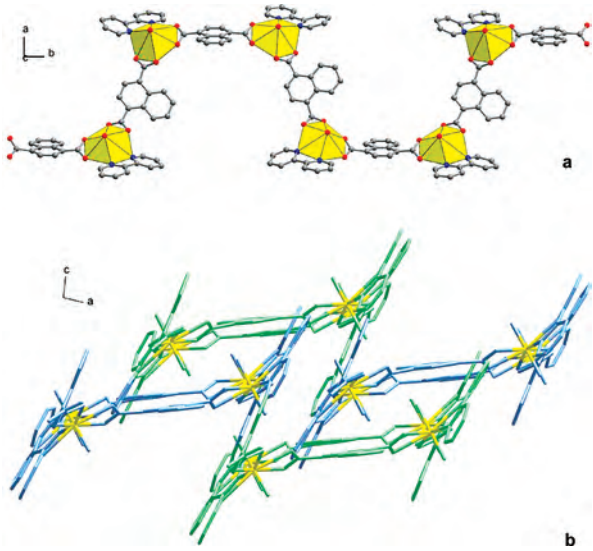

Figure 8. One uranyl−organic chain in **3** viewed along the *c* axis (a) and the packing of the chains viewed along the *b* axis (b).

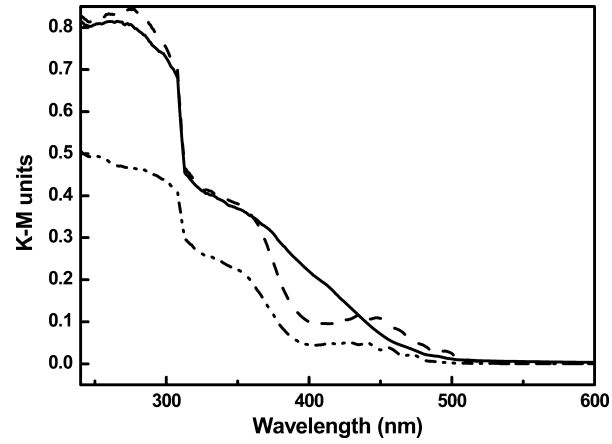

Figure 9. UV/vis diffuse-reflectance spectra of **1** (solid), **2** (dash), and **3** (dash-dot).

the uranyl units prefer O-donors to N-donors.[23] This follows the hard/soft acid/base (HSAB) theory. U(VI) is a relative "hard" acid, and therefore, it tends to bond to the O-donors, the "hard" base. The N-donor, on the other hand, is more likely to bond the softer transition metal ions if available, as in **2**.[13,14,24] However, the bonding between U and N is still possible.[25] This indicates that the boundary between hard and soft is not absolute, and the HSAB consideration is not the only factor to determine the coordination. More importantly, when extended frameworks are concerned, other factors should also be taken into account. Sterics, for example, as discussed by Cahill et al.,[26] could be essential in determining the binding fashion of uranyl centers and may significantly contribute to the coordination for chelating N-containing ligands. Also, the interaction between ligands cannot be neglected. As in **3**, besides the chelation effect, the face-to-face π-π stacking between bipy and NDC aromatic rings may contribute to the stabilization of the binding between 2,2′-bipy and uranyl units.

Photocatalytic activity is an attractive property of uranyl compounds.[14] To elucidate the photoresponse wavelength region, the solid state diffuse-reflectance UV/vis spectra for the as-synthesized compounds were recorded and are presented in Figure 9. Typical UV/vis spectra of uranyl compounds usually consist of absorption components in the UV and visible region. The former arises from charge transfer electronic transition within the U═O double bonds,[27] which is proven to be responsible for uranyl photocatalytic activities while the latter is attributed to ligand to metal charge transfer (LMCT) between the O (or N) atoms of the coordinating ligands and an empty orbital of the U(VI) ions.[28] Compounds **2** and **3** show such typical spectra with strong charge-transfer absorptions below 400 nm and LMCT absorptions in the region from 410 to 520 nm while for compound **1** the two

(23) Thuéry, P. *Inorg. Chem.* **2007**, *46*, 2307–2315.
(24) Wang, C. M.; Liao, C. H.; Kao, H. M.; Lii, K. H. *Inorg. Chem.* **2005**, *44*, 6294–6298.
(25) (a) Thuéry, P. *Eur. J. Inorg. Chem.* **2006**, 3646–3651. (b) Jiang, Y. S.; Li, G. H.; Tian, Y.; Liao, Z. L.; Chen, J. S. *Inorg. Chem. Commun.* **2006**, *9*, 595–598.
(26) Frisch, M.; Cahill, C. L. *Dalton Trans.* **2006**, 4679–4690.
(27) (a) Volkovich, V. A.; Griffiths, T. R.; Fray, D. J.; Thied, R. C. *Phys. Chem. Chem. Phys.* **2001**, *3*, 5182–5191. (b) Almond, P. M.; Albrecht-Schmitt, T. E. *Inorg. Chem.* **2002**, *41*, 1177–1183.
(28) (a) Addleman, R. S.; Carrott, M.; Wai, C. M.; Carleson, T. E.; Wenclawiak, B. W. *Anal. Chem.* **2001**, *73*, 1112–1119. (b) Huang, J.; Wang, X. Q.; Jacobson, A. J. *J. Mater. Chem.* **2003**, *13*, 191–196.

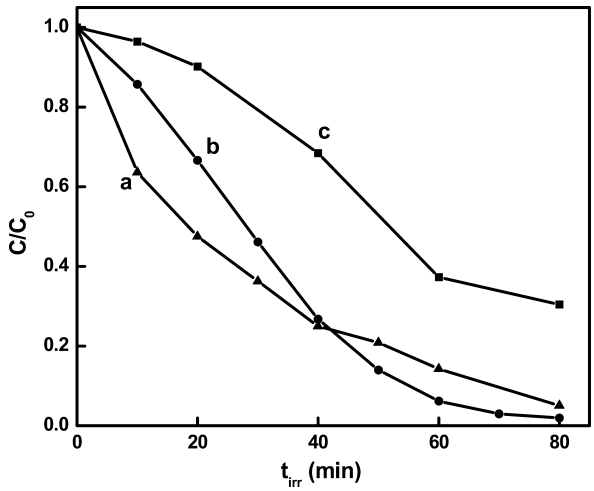

Figure 10. Concentration changes of RhB irradiated with UV light as a function of time t_{irr} in the presence of **1** (a), **2** (b), or without any catalyst (c).

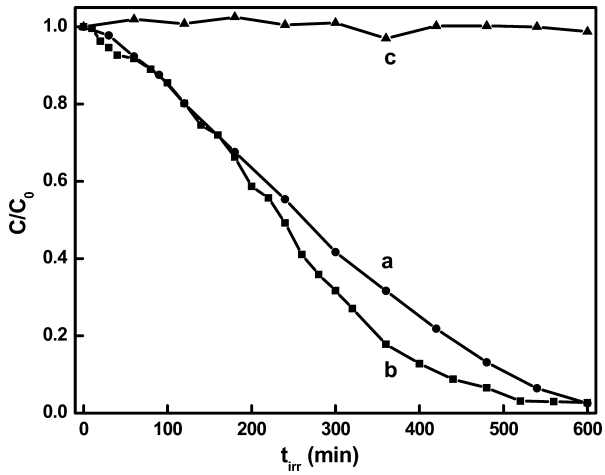

Figure 11. Concentration changes of RhB irradiated with visible light as a function of time t_{iir} in the presence of **1** (a), **2** (b), or without any catalyst (c).

proportions of absorption overlap each other. It should be noticed that the absorption onset of the photoexcitation of the U═O double bonds for **2** occurs in the visible region, indicating that they may be photocatalytically active upon visible irradiation, whereas for **1**, although the overlap of the two absorption components in the spectrum renders such consideration ambiguous, the photocatalytic activity upon visible light excitation is proven experimentally.

Compounds **1** and **2** have been tested for photocatalytic degradation of RhB which is regarded as a molecule difficult to degrade.[29] It was not possible to evaluate the photocatalytic performance of compound **3** because of its extreme low yield. Photocatalytic results are presented in Figures 10 and 11. Both **1** and **2** show similar activities under UV or visible light irradiation, and they are able to degrade RhB efficiently. When UV light was applied, the self-degradation of RhB complicated the assessment of the uranyl catalytic performance, and therefore Xe lamp irradiation (visible light) was

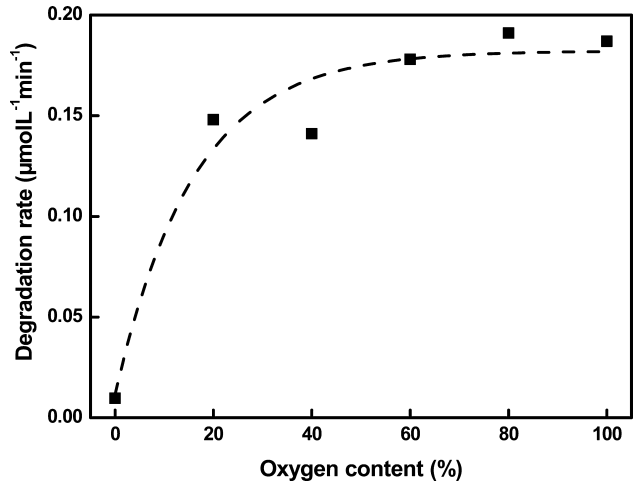

Figure 12. Degradation rate of RhB versus oxygen content in the bubbling gas and the fit of the plot.

used to evaluate the photocatalytic activities of the samples. Under Xe irradiation, the degradation curves demonstrate the distinct photocatalytic activities of **1** and **2**, and the RhB is degraded almost completely in 10 h of irradiation.

The photocatalytic properties for uranyl ions in aqueous solutions have been well documented in the literature,[30] whereas there have been very few reports about photocatalysis of uranyl-containing solids. Previously, we demonstrated the photocatalytic activities of uranyl-containing solid compounds for organic dye degradation.[14] In this work, we are able to compare the photocatalytic performances of two structurally similar compounds with and without a second metal ion in the structure. The presence of $Ag(2,2'\text{-bipy})_2^+$ in **2** makes the comparison possible. Furthermore, in contrast to Ni^{2+} and Zn^{2+}, Ag^+ is sensitive to light, rendering it more important to clarify whether or not the Ag species contributes to the photocatalytic activity. Because **1** and **2** are similar in uranium content (33.6% for **1** and 30.9% for **2**), and both possess a 2D layered structure with similar accessibility to active uranyl centers, the similarity in photocatalytic performance for these two compounds suggests that the uranyl units are the ones responsible for the catalytic properties, whereas the Ag species are of less importance. However, it should be pointed out that the possibility to tune the catalytic properties of uranyl-containing materials by assembling other metal ions or nonmetal species is not excluded.[31] To rule out the possibility that the photocatalytic activity of **1** and **2** arises from molecular or oligomeric species formed through dissolution of the solid samples in the photocatalytic reaction systems, control experiments were conducted. We filtered the reaction suspensions after 10 h of irradiation to remove the solid catalyst, and fresh RhB was added into the respective filtrates for catalysis testing. Without solid catalyst in the reaction system, the RhB was not degraded in 10 h of irradiation under a Xe lamp, suggesting that the solution contains no photocatalytically active species. Furthermore, the characteristic UV/vis absorptions of the uranyl units were

(29) Ma, W. H.; Li, J.; Tao, X.; He, J.; Xu, Y. M.; Yu, J. C.; Zhao, J. C. *Angew. Chem., Int. Ed.* **2003**, *42*, 1029–1032.

(30) Burrows, H. D.; Kemp, T. J. *Chem. Soc. Rev.* **1974**, *3*, 139–165.

(31) Sarsfield, M. J.; Helliwell, M. *J. Am. Chem. Soc.* **2004**, *126*, 1036–1037.

Scheme 1. Major Oxygen Consumption Steps Involved in the RhB Degradation Process

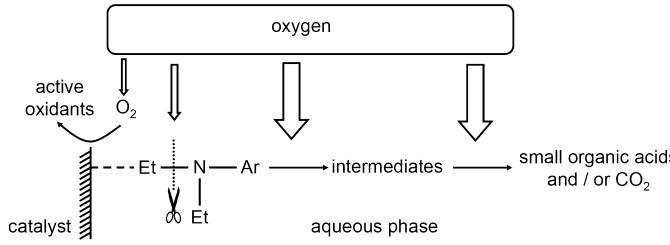

not observed when recording the absorption spectra of the RhB solutions after photocatalytic reactions. This means that the concentration of the molecular and/or oligomeric species dissolved from solid **1** and **2** in the photocatalytic reaction systems is, if any, negligible. Therefore, it is believed that the photocatalytic activity for the system containing **1** or **2** as the catalyst arises from the solid compound.

The photocatalytic reaction mechanism is another aspect for consideration to optimize the materials for practical applications. Two important mechanisms, H-abstraction and electron transfer, have been proposed for uranyl catalyzed photo-oxidation of organic compounds.[32] These mechanisms were for UO_2^{2+} cations in solutions, but they may also be suitable for solid uranyl coordination compounds as the same active uranyl centers are involved. Previously, we investigated the photoexcitation, electron transfer, and recovery of uranyl centers and the degradation pathways of the RhB molecules catalyzed by uranyl compounds.[14] However, the impact of oxygen on the photocatalytic degradation reaction was not addressed, although the presence of oxygen was proven to be essential. The linear fits of the plots of RhB concentration versus reaction time under visible irradiation (Supporting Information, Figure S5) indicate that the RhB degrades at a constant rate for the first 3 h for all the oxygen contents. This is easily understood for a heterogeneous catalytic reaction, because when the reactant (RhB in this case) is excessive, the reaction rate solely depends on the amount of active centers of the catalyst. By controlling the oxygen concentration in the bubbling gas, we can elucidate the correlation between catalytic reaction rate and oxygen concentration because the oxygen concentration in an aqueous solution is proportional to its pressure in the purging gas. A xenon lamp was used to avoid RhB self-degradation which would make the quantitative analysis inaccurate. In addition, because of the similar activity of **1** and **2**, only **1** was used for the degradation assessment. As shown in Figure 12, the plot of the RhB degradation rate versus oxygen concentration is not linear. Initially, the rate rises sharply with increase of oxygen concentration. This is not surprising because the oxygen molecules serve to capture the excited electrons in the uranyl LUMO orbitals, generating highly active species (most possibly H_2O_2 or O_2^-) which can oxidize RhB readily. The higher the oxygen concentration, the more the subsequently generated active oxidation species in the reaction system. In addition, the molecular oxygen itself is also an oxidant for the oxidation of the generated organic intermediates. As the oxygen concentration increases further, the slope of the curve in Figure 12 decreases gradually. For example, when the oxygen content rises from 0% to 20%, the degradation rate is increased from 0 to approximately 0.14 μmol L^{-1} min^{-1}, whereas when the oxygen content rises from 20% to 100%, the reaction rate is enhanced only by 35% (approximately from 0.14 to 0.19 μmol L^{-1} min^{-1}). In other words, the photocatalytic degradation rate is very sensitive to O_2 at low oxygen contents but appears to be saturated upon increasing the oxygen content to a certain value. This observation is consistent with the cracking mechanism of RhB in photocatalytic reactions. As elucidated previously, the degradation of RhB occurs both on the surface of the catalyst and in the solution. The RhB itself is stable to O_2 and visible light. Once associated with photoexcited uranyl centers, the degradation of RhB starts with H-abstraction and stepwise de-ethylation in association with photoexcited uranyl centers to generate active intermediates, which are further cracked by the oxygen-centered species in the solution, ending up with small organic acids and CO_2 (Scheme 1).[14,33] Most of the degradation steps involve redox reactions and demand O_2 (and/or H_2O_2, O_2^-, etc.). Therefore, all the reaction steps in the whole degradation process are in competition for oxygen consumption. The photoexcited uranyl species associated with abstracted RhB molecules tend to capture O_2 (and/or H_2O_2, O_2^-, etc.) most easily, giving rise to the sharp increase of degradation rate in Figure 12. However, the formation of the RhB-associated photoexcited uranyl centers is slow, and if the O_2 concentration continues to rise, the amount of RhB molecules that are associated with the excited uranyl units is not sufficient to react with the O_2 (and/or H_2O_2, O_2^-, etc.) present in the system. As a result, the decrease rate of the RhB concentration monitored through UV/vis spectroscopy is not linearly proportional to, but lags behind the rise of the oxygen concentration in the reaction system.

Conclusions

By employing NDC and bipyridine ligands, we have successfully accommodated uranyl units into three novel coordination assemblies (compounds **1**, **2**, and **3**). **1** and **2** consist of 2D infinite uranyl−organic layers constructed from

(32) (a) Matsushima, R.; Sakuraba, S. *J. Am. Chem. Soc.* **1971**, *93*, 7143–7145. (b) Matsushima, R. *J. Am. Chem. Soc.* **1972**, *94*, 6010–6016. (c) Bakac, A.; Espenson, J. H. *Inorg. Chem.* **1995**, *34*, 1730–1735. (d) Wang, W. D.; Bakac, A.; Espenson, J. H. *Inorg. Chem.* **1995**, *34*, 6034–6039. (e) McCleskey, T. M.; Burns, C. J.; Tumas, W. *Inorg. Chem.* **1999**, *38*, 5924–5925.

(33) Horikoshi, S.; Saitou, A.; Hidaka, H.; Serpone, N. *Environ. Sci. Technol.* **2003**, *37*, 5813–5822.

U−O polyhedra and NDC molecules. The apertures within the layers are packed into channels, in which are located 4,4′-bipyridine for **1** and $[Ag(2,2'\text{-bipy})_2]^+$ for **2**, respectively. It is unusual that both tetranuclear U−O clusters and mononuclear uranyl units are found in **2**. In **3** both NDC and 2,2′-bipyridine coordinate to uranium centers to form 1D zigzag chain structures. In **1** and **2**, the N-donors do not coordinate to uranyl centers, following the prediction of hard/soft acid/base (HSAB) theory. Whereas in **3**, the coordination between uranyl and 2,2′-bipy suggests that besides HSAB consideration, other factors such as sterics and interligand interactions also affect the coordination behavior of the ligands, especially when extended structures are formed. Under UV or visible irradiation, both **1** and **2** degrade RhB with similar efficiency, indicating that the photocatalytic activity is solely attributed to the uranyl centers in the compounds, whereas the Ag species is less important in the photocatalytic reaction process. Further investigation demonstrates that the increase of the photocatalytic degradation rate lags behind the oxygen concentration rise.

Acknowledgment. This work was financially supported by the National Basic Research Program (2007CB613303) and the National Natural Science Foundation of China.

Supporting Information Available: XRD patterns, selected bond lengths and angles, crystallographic data in CIF format, plots of RhB degradation rate versus reaction time in the presence of **1** at various O_2 contents, and layout of the photocatalytic reaction vessel (PDF). This material is available free of charge via the Internet at http://pubs.acs.org.

IC800109Y